International Journal of Rotating Machinery, 9(2): 127–133, 2003

1023-621X/03 $12.00 + .00
DOI: 10.1080/10236210390147470

Taylor & Francis
Taylor & Francis Group

Mechatronical Design Studies on Small Brushless Motors

W. Amrhein, S. Silber, K. Nenninger, and G. Trauner
LCM—Linz Center of Competence in Mechatronics at Johannes Kepler University, Linz, Austria

R. Schöb
Levitronix GmbH, Zurich, Switzerland

Brushless DC- and AC-permanent-magnet motors controlled by powerful micro-controller electronics have opened up a significant share of the small motor market in the last years. Based on the mechanical low cost construction of a single-phase motor the paper presents electronic drive concepts to improve the performance and for special applications also the lifetime of brushless motors. The tangential and radial forces acting on the rotor are controlled by special phase current curves to reduce the torque ripple and to avoid expendable machinery parts like ball or sliding bearings.

Keywords bearingless motors, operation performance, radial forces, single-phase motors, torque

During the last ten years the economical and technical [1]importance of brushless DC and AC permanent-magnet drives has considerably increased in the field of small drive technology. The strong industrial competition and high technical demands lead to new customer and cost oriented drive solutions. The variety ranges from simple single-phase motors for fans or blowers to advanced servo drive systems for superior control applications. Whereas in the past complex drive functions have been accompanied by expensive mechanical constructions, today we have a strong trend to low cost mechanics combined with microprocessor-controlled electronics to get excellent motor performances.

To show the impressive possibilities of modern electronics controlled by powerful micro-controllers the paper presents an electronic method for torque ripple compensation and a method for the control of radial forces to allow a high-performance bearingless motor operation. The analysis are based on the principle of a single-phase motor with a four coil arrangement in the armature.

Received 28 March 2002; accepted 28 March 2002.
Address correspondence to Wolfgang Amrhein, LCM—Linz Center of Competence in Mechatronics at Johannes Kepler University of Linz, Altenbergerstrasse 69, A-4040 Linz, Austria. E-mail: amrhein@mechatronics.uni-linz.ac.at

OPTIMAL OPERATION CURRENTS FOR SMALL SINGLE-PHASE MOTORS

In the fan and blower industry four pole single-phase permanent-magnet motors are frequently used for cooling and climate applications. Owing to their single-phase voltage or current feeding these motors only allow the generation of magnetic alternating fields by the change of the direction of the armature current. Therefore special measures have to be taken to guarantee a reliable start from all rotor angle positions. One possible measure is an asymmetrical design of the ferromagnetic poles as shown in Figure 1. According to the asymmetrical air gap the cogging torque

$$T_{\text{cog}}(\varphi) = \frac{\partial W_{\text{coen}}(\theta_p, \varphi)}{\partial \varphi} \qquad [1]$$

acting on the permanent-magnets moves the rotor to a start position, where the magnetic coenergy W_{coen} becomes a maximum. The cogging torque presented in Figure 2 is independent from current as long as the ferromagnetic material shows a linear characteristic.

The second component the electromagnetic torque can be directly controlled by the phase currents and is generally defined by

$$T_{\text{el}}(\varphi) = \sum_{k=1}^{m} \frac{d\Psi_{p_k}(\varphi)}{d\varphi} i_k + \frac{1}{2} \sum_{k=1}^{m} \sum_{i=1}^{m} \frac{dL_{ki}(\varphi)}{d\varphi} i_i i_k, \qquad [2]$$

whereas m denotes the phase number, ψ_{pk} the flux linkage of the armature with the permanent-magnet field and L_{ki} the self- and mutual inductances.

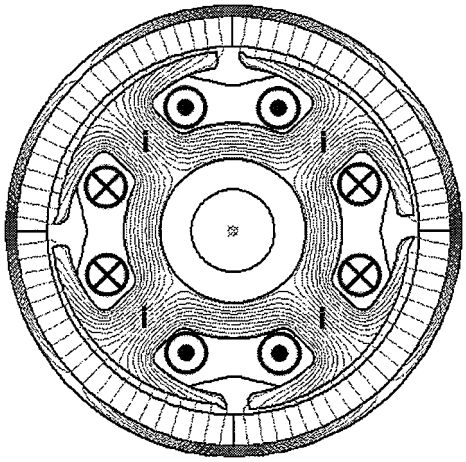

FIGURE 1
Conceptional design of the single-phase permanent-magnet motor (field distribution for $i = 0$).

In the special case of the single-phase motor equipped with a circular permanent-magnet and ferromagnetic joke arrangement in the rotor (see Figure 1.) the following simplifying conditions are valid:

$$m = 1 \tag{3}$$

$$\frac{dL_{ki}}{d\varphi} = 0. \tag{4}$$

Typically the overall torque curves of single-phase motors have high torque ripple values as shown in Figure 2. One possibility to smooth the overall torque of the motor for a special stationary operation point is to tune the cogging torque and electromagnetic torque curves by optimized permanent-magnet and armature designs. However measures like skewed permanent-magnet segments, increased air gaps or chorded windings lead to inevitable torque reductions and therefore are very unpopular.

Better results concerning the leakage of torque can be achieved by an electronic torque compensation method supposed in the following.

Assuming a motor design complying with condition (4) and generating a cogging torque curve where the maximum value corresponds with the stationary torque operation point T_{oper} of the application the necessary electromagnetic torque for smooth performance can be generally described by

$$T_{\text{el}}(\varphi) = \sum_{k=1}^{m} \frac{d\Psi_{p_k}(\varphi)}{d\varphi} i_k = T_{\text{oper}} - T_{\text{cog}}(\varphi) \tag{5}$$

provided that the magnetic circuit has a linear ferromagnetic characteristic. With the additional condition

$$P_v = \sum_{k=1}^{m} R_k i_k^2(\varphi) = \min \tag{6}$$

for minimal copper losses in the motor windings and the following formulation using the Lagrange multiplicator λ

$$\frac{\partial P_v}{\partial i_k} - \lambda \frac{\partial T_{\text{el}}}{\partial i_k} = 0 \tag{7}$$

the equation system for an independent current control of k phases can be derived:

$$i_k(\varphi) = T_{\text{el}} \frac{d\psi_k}{d\varphi} \left(R_k \sum_{\kappa=i}^{m} \frac{\left(\frac{d\psi_\kappa}{d\varphi}\right)^2}{R_\kappa} \right)^{-1}. \tag{8}$$

For a single-phase operation the current Equation (8) simplifies to

$$i(\varphi) = T_{\text{el}} \left(\frac{d\psi}{d\varphi} \right)^{-1}. \tag{9}$$

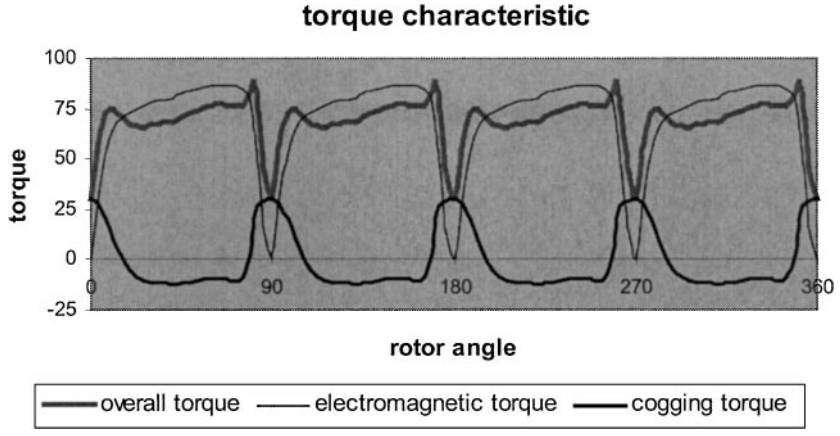

FIGURE 2
Different torque components of a single-phase permanent-magnet motor with an asymmetrical ferromagnetic pole design.

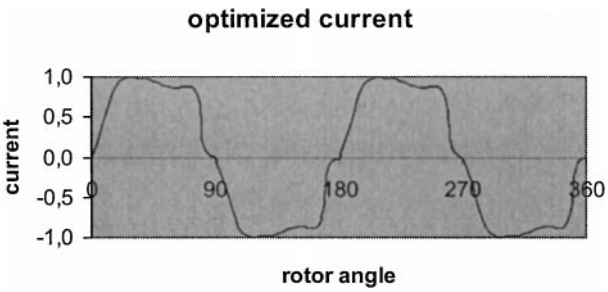

FIGURE 3
Optimized current curve for smooth torque performance.

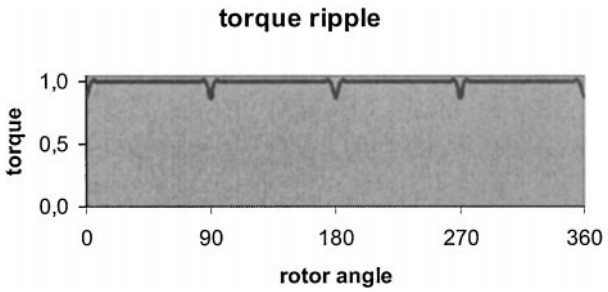

FIGURE 5
Torque ripple for clipped current values according to Figure 4.

Figure 3 shows the corresponding calculated current waveform for a motor operation with smooth torque performance. To get a high quality of torque performance two conditions should be complied with: the maximum of the cogging torque should match with the value of the stationary load torque and the maximum should also be in phase with the zero point of the electromotive force. A bad adaptation can lead to extreme high current peaks in the region of low electromotive force values. Figure 4 shows the effects on the resulting current waveform caused by a supposed phase-shift of the cogging curve of 7.5 degrees and an additional amplitude deviation of 5%. The resulting current transients in Figure 4 have amplitudes many times over the average amplitude and therefore have to be limited by the current controller. The influence of the current limitation in Figure 4 on the corresponding torque performance is illustrated in Figure 5. As the derivation of the flux linkage is nearly zero in these regions, a complete elimination of the current peaks of Figure 4 hardly influences the torque curve of Figure 5 and results in better noise values.

ADDITIONAL RADIAL FORCE GENERATION FOR BEARINGLESS MOTOR OPERATION

Up to now the four coils of the brushless single-phase motor have been connected in serial or parallel. In the case of disconnection the currents can be impressed independently in each coil.

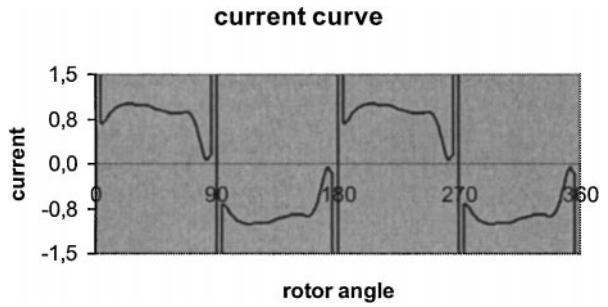

FIGURE 4
Current curve for a non adapted cogging torque curve (current peaks clipped).

This measure leads to additional degrees of freedom to control the rotor position not only in angular but also in orthogonal d- and q-directions of the rotor plane.

The radial forces on the four pole permanent-magnet rotor can be controlled by superimposed magnetic fields whose pole pair numbers differ from the permanent-magnet pole pair number by 2 [1, 2].

For a better understanding of the machine, it is appropriate to start first with the winding arrangement of Figure 6. The winding system of a magnetic bearing component and the single phase motor component are arranged separately in the machine slots. The two phases of the magnetic bearing component fed by the currents i_1 and i_2 generate a two pole rotatory field responsible for the control of radial forces. The third phase supplied with the current i_3 is equipped with four poles corresponding to the pole number of the permanent-magnet rotor. It produces the motor torque by an alternating field as in the example before. The linkage flux of the three phases can be described by the rotor angle and rotor position depending inductances L_{ij} and the permanent-magnet flux components ψ_{pi}.

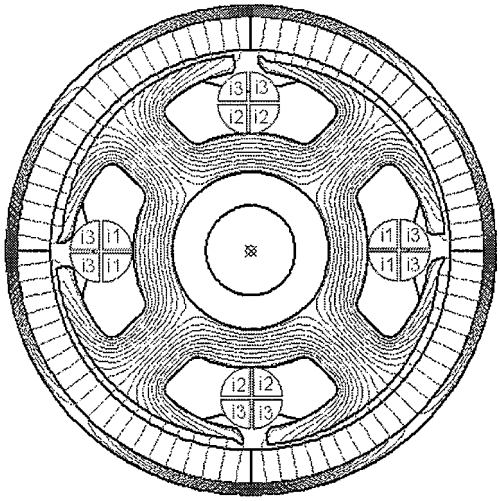

FIGURE 6
Auxiliary three-phase design for an independent torque and radial force control.

With the flux linkage of the armature with the permanent-magnet field

$$\psi_p = \begin{bmatrix} \psi_{p1} \\ \psi_{p2} \\ \psi_{p3} \end{bmatrix}, \qquad [10]$$

the inductance matrix of the motor

$$\Lambda = \begin{bmatrix} L_{11} & 0 & L_{13} \\ 0 & L_{22} & L_{23} \\ L_{31} & L_{32} & L_{33} \end{bmatrix}, \qquad [11]$$

and the phase current vector

$$i_{\mathrm{III}} = \begin{bmatrix} i_1 \\ i_2 \\ i_3 \end{bmatrix} \qquad [12]$$

the total armature flux linkage becomes

$$\psi = \psi_p + \Lambda i_{\mathrm{III}}. \qquad [13]$$

L_{12} and L_{21} have zero values due to the orthogonal position of the magnetic bearing phases 1 and 2. L_{13}, L_{23}, L_{31} and L_{32} are mutual inductances between the two pole and the four pole winding system.

For linear conditions the magnetic energy and the magnetic coenergy respectively are equal and can be defined by the equation

$$W_{\mathrm{mag}} = \frac{1}{2} i_{\mathrm{III}}{}^T (\psi_p + \Lambda i_{\mathrm{III}}). \qquad [14]$$

The mmf distribution of the stator in Figure 6 can also be realized by the four coil winding arrangement of Figure 7. Each coil represents one independent phase. With the transformation matrix

$$\Gamma = \begin{bmatrix} 1 & -1 & -1 \\ 1 & 1 & 1 \\ -1 & 1 & -1 \\ -1 & -1 & 1 \end{bmatrix} \qquad [15]$$

and the current vector of the four phase model according to Figure 7

$$i_{\mathrm{IV}} = \begin{bmatrix} i_a \\ i_b \\ i_c \\ i_d \end{bmatrix}, \qquad [16]$$

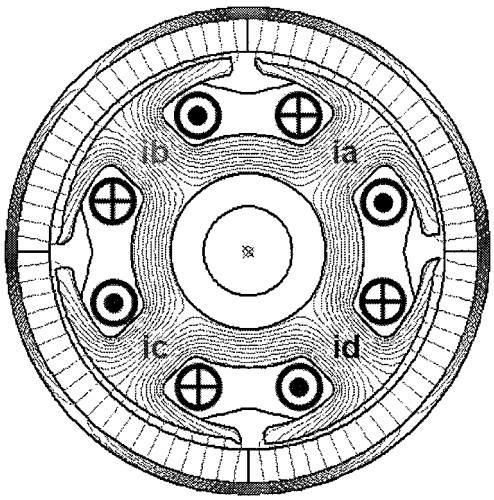

FIGURE 7
Motor with four independent phases for bearingless motor control.

the transformation condition for the two systems results in

$$i_{\mathrm{IV}} = \Gamma i_{\mathrm{III}}. \qquad [17]$$

The formulation of W_{mag} in (14) can be modified using the current definition of the four phase arrangement of Figure 7

$$W_{\mathrm{mag}} = \frac{1}{2} \left[\Gamma^{-1} i_{\mathrm{IV}} \right]^T \left[\psi_p + \Lambda \Gamma^{-1} i_{\mathrm{IV}} \right]. \qquad [18]$$

Finally we get the expression for calculating the radial forces and the torque by the partial differentiations of W_{mag}

$$\begin{bmatrix} F_x \\ F_y \\ T \end{bmatrix} = \begin{bmatrix} \partial W_{\mathrm{mag}}/\partial x \\ \partial W_{\mathrm{mag}}/\partial y \\ \partial W_{\mathrm{mag}}/\partial \delta \end{bmatrix}, \qquad [19]$$

where x and y denote the Cartesian coordinates in d- and q-direction and δ the rotor moving angle.

The phase currents necessary for force and torque control of the bearingless motor can be calculated from Equations (18) and (19). Figure 8 illustrates the angle dependent course of the forces in the d- and q-direction at constant phase currents. The results of this diagram are achieved by feeding only one phase each time.

With the control of the phase currents of vector $i_{\mathrm{IV}}$the rotor position is actively stabilized in three degrees of freedom. The remaining degrees of freedom can be stabilized either by additional axial magnetic bearings or as suggested in Figure 9 passively by the axial reluctance forces of the magnetic circuit.

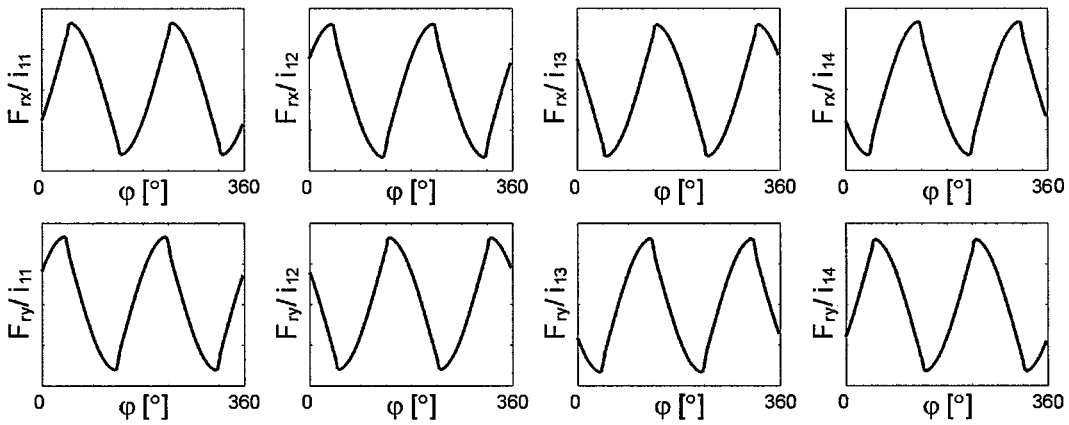

FIGURE 8
Curves of radial forces in the d- and q-direction at constant phase currents (phases are separately fed).

MEASUREMENTS

The following figures present some measurements concerning the bearingless motor characteristics. Figure 10 shows the course of the orbit curves of the test motor up to its nominal speed. The excursions are mainly caused by an high unbalance of the exterior rotor. The maximum excursion at nominal speed is about 20% of the motor air gap. This value can be significantly improved by either a mechanical balancing of the rotor or—less expensive—by the implementation of an electronic unbalance compensation which moves the rotation axis to the mass centroid axis of the rotor.

Figure 11 shows a simulation and measurement comparison of the rotor response when a step function

$$F_x(t) = (-0.1 + 0.2\sigma(t))F_{x\max} \qquad [20]$$

of the radial force is applied to the rotor.

In Equation (20) the step function is defined by

$$\sigma(t) = 0 \text{ for } t < 0$$

and

$$\sigma(t) = 1 \text{ for } t \geq 0. \qquad [21]$$

The radial force step function of Equation (20) is internally generated by the superposition of the regular stator phase currents with transient disturbance current components. Both the maximum amplitude of the rotor movement and the course of the transient response show good accordance between simulation and measurement. In addition Figure 11 shows that the force functions can be considered as widely decoupled concerning the responses in the x- and y-axis of the rotor plane.

APPLICATIONS

The motor presented above is based on an alternating field motor concept equipped with the additional integrated facility to generate levitation forces for a bearingless motor operation. For the reason of the single-phase concept the motor is only appropriate for applications which don't need a very high starting

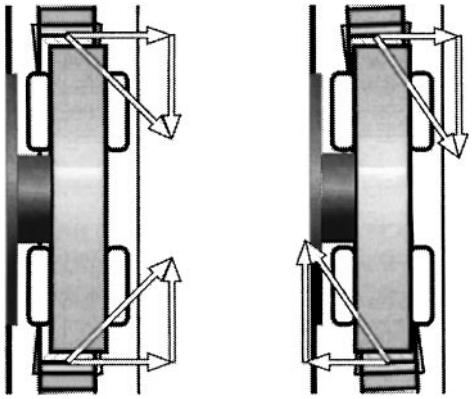

FIGURE 9
Passive stabilization of the rotor position in three degrees of freedom by reluctance forces.

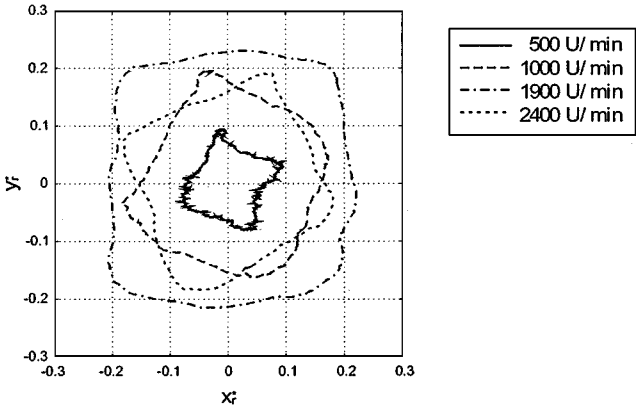

FIGURE 10
Orbit curves of the exterior rotor at several speeds.

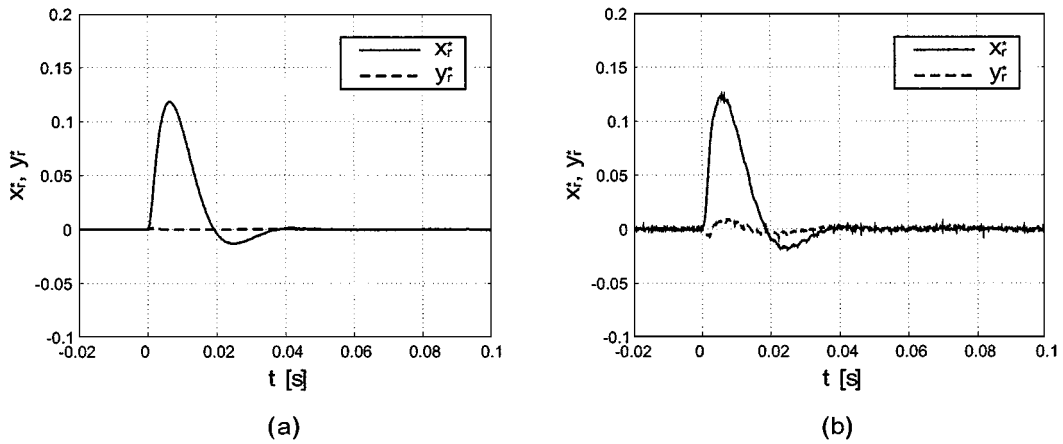

FIGURE 11
Radial rotor movement corresponding with the step function of Equation (20): (a) Simulation and (b) Measurement.

torque. Applications which meet these requirements are for instance fans, blowers, ventilators or pumps.

Figure 12 illustrates a pump concept where the bearingless motor is an integral component of the pump device. The magnetic rotor forces necessary for torque and position control are generated by air gap fields penetrating the non ferromagnetic pump housing. The main advantage of this motor concept are the lack of mechanical bearings and shaft seals.

CONCLUSION

Beside mechanical design considerations the motor supply with optimized current waveforms controlled by microprocessors could be of major importance in the future brushless permanent-magnet motor technology. Two electronic measures for the improvement of the performance of brushless permanent-magnet motors concerning torque ripple and lifetime are presented in this paper. Using the Lagrange multiplicator the optimal angle dependent current curves for low copper losses have been calculated for the advanced operation of a single-phase permanent-magnet motor.

Furthermore the paper deals with the calculation and generation of radial forces and their corresponding currents in order to stabilize the rotor position in two additional degrees of freedom without the necessity of mechanical ball or sliding bearings. A stand alone operation of the motor without mechanical or magnetic bearings is facilitated by a suitable combination of active and passive stabilization measures.

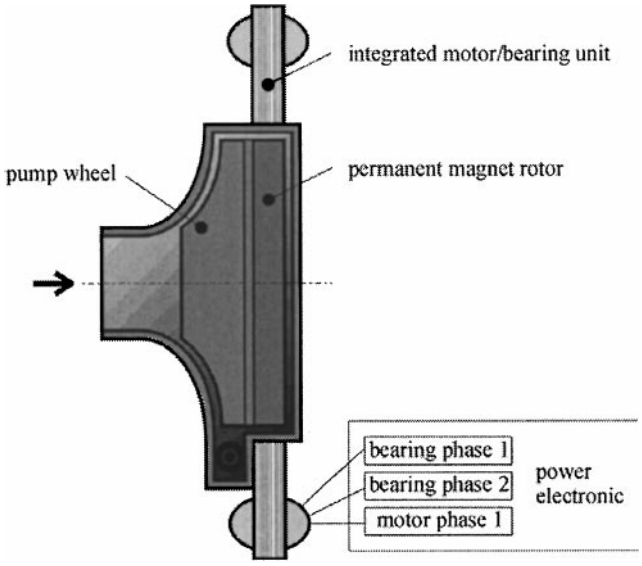

FIGURE 12
Pump concept based on the integration of a bearingless permanent-magnet motor.

ACKNOWLEDGMENTS

The development of bearingless drives is a project of the ‘Linz Center of Competence in Mechatronics’ as a part of the Kplus-program of the Austrian government. The project is kindly supported by Levitronix GmbH Zurich, Levitec GmbH, Lahnau, the Austrian and Upper Austrian government and the Johannes Kepler University of Linz. The authors thank all involved partners for their support.

REFERENCES

Bichsel, J. 1990. Beiträge zum lagerlosen Elektromotor. Ph.D. diss., ETH Zurich.

Schöb, R. 1993. Beiträge zur lagerlosen Asynchronmaschine. Ph.D. diss., ETH Zurich.

Schöb, R., and Bichsel, J. 1994. Vector control of the bearingless motor, 327–332. *Proceedings of the 4th International Symposium on Magnetic Bearings*. Zurich, Switzerland: August 23–26.

Ohishi, T., Okada, Y., and Dejima, K. 1994. Analysis and design of a concentrated wound stator for synchronous-type levitated motor,

201–206. *Proceedings of the 4th International Symposium on Magnetic Bearings*. Zurich, Switzerland: August 23–26.

Oshima, M., Miyazawa, S., Deido, T., Chiba, A., Nakamura, F., and Fukao, T. 1996. Characteristics of a permanent-magnet type bearingless motor, 363–370. *IEEE Transactions on Industrial Applications, Vol. 32, No. 2*, March/April.

Schweitzer, G., Bleuler, H., and Traxler, A. 1994. Active magnetic bearings, vdf-verlag, Zurich.

Barletta, N. 1998. Der lagerlose Scheibenmotor. Ph.D. diss., ETH Zurich.

Silber, S. 2000. Beiträge zum lagerlosen Einphasenmotor, Ph.D. diss., Linz University.

Amrhein, W., and Silber, S. 1998. Bearingless single-phase motor with concentrated full-pitch windings in interior rotor design, 486–496. *Proceedings of the 6th International Symposium on Magnetic Bearings*, Cambridge, Massachusetts, USA: August 5–7.